

Ag-Pd 纳米合金低温连接及其抗电化学迁移性能

贾强, 王文淦, 阿占文, 邓钟炆, 冯斌, 刘磊*

清华大学机械工程系, 摩擦学国家重点实验室, 北京 100084

摘要 纳米银焊膏能够实现低温连接、高温服役,同时具有优异的导电、导热性能,其缺点是非常容易发生电化学反应。本文采用脉冲激光沉积成功制备了完全互溶的 Ag-10%Pd 纳米合金,并将其用于 SiC 芯片的封装互连,旨在提高纳米颗粒烧结层的抗电化学迁移能力,同时保持纳米颗粒的低温烧结特性。研究表明,采用 Ag-10%Pd 纳米合金烧结连接 SiC 芯片及镀银的直接覆铜基板(DBC),在 250 °C 的温度下可以实现剪切强度为 21.89 MPa 的接头,达到了美国军标 MIL-STD-883K 的要求(7.8 MPa)。Ag-Pd 纳米合金抗电化学迁移能力是同等条件下纯银的 4.3 倍。在 Ag-Pd 纳米合金中,银离子的析出受到 PdO 的阻碍,迁移产物呈云雾状分布,有效延长了电极的短路时间。脉冲激光沉积 Ag-Pd 纳米合金的烧结避免了传统银、钯颗粒直接混合方法后续高达 850 °C 的合金化过程。Ag-Pd 纳米合金作为封装互连材料是实现低温连接的有效保证,并有望为功率电子器件的高可靠性封装提供解决方案。

关键词 激光技术; 纳米合金; 低温烧结; 电子封装; 电化学反应

中图分类号 TH142.2

文献标志码 A

doi: 10.3788/CJL202148.0802014

1 引言

随着第三代功率半导体器件的发展,以 SiC 为代表的宽禁带半导体芯片在大功率电力电子器件中扮演着越来越重要的角色,并逐渐替代了传统的硅芯片。然而,与传统硅芯片配套的芯片封装材料却难以在高温下持久服役,成为 SiC 功率电子器件应用的短板^[1-3]。人们迫切需要一种能够低温连接、高温服役的封装互连材料,因而纳米颗粒焊膏烧结技术应运而生。纳米银焊膏因连接温度低和具有优异的导电、导热性能,已成为宽禁带半导体芯片封装领域的研究热点^[4-5]。然而,银是最容易发生电化学反应的金属之一,尤其是在高温、高湿环境下,阳极失去电子后,银离子迁移至阴极并不断沉积,最终导致器件短路失效^[6-7]。功率电子器件的功率密度越来越高,工作温度也越来越高,尤其是一些高功率电子器件,其工作环境更为恶劣,极大地限制了烧结银在功率电子器件中的可靠应用。

钯被认为是改善银抗电化学反应能力最有效的金属之一^[8]。目前,一些国外公司(例如 Panasonic、ADATA)已经采用钯来提高含银电阻的抗电化学反应能力。早在 1979 年,Naguib 等^[9]就采用水滴试验研究了添加不同含量的钯对银抗电化学反应能力的影响,结果表明,当钯的质量分数达到 19%时,银的迁移速率降低为原来的 1/100。Lin 等^[10]研究了钯抑制银迁移的机理,并指出 PdO 的生成抑制了银在阳极的溶解。天津大学的王迪^[11]向纳米银焊膏中添加了质量分数为 15%的纳米钯颗粒(粒径为 50~100 nm),结果发现,烧结层抗电化学反应的能力由于钯的氧化而得到了明显改善。目前,添加钯的形式大多为银、钯颗粒直接混合,这种方法后续需要高达 850 °C 的合金化温度。如果二者的合金化不够充分,就会影响烧结层的致密化,同时也会带来较高的电阻等一系列问题^[12]。然而,如此高的合金化温度用于功率电子器件的封装显然是不能被接受的^[13-14]。如果能直接制备 Ag-Pd 纳米合金颗粒,就

收稿日期: 2020-11-30; 修回日期: 2020-12-24; 录用日期: 2021-01-20

基金项目: 国家重点研发计划专项(2017YFB1104900)、国家自然科学基金(51775299,52075287,51520105007)

* E-mail: liulei@tsinghua.edu.cn

可以避免烧结过程所需要的高温合金化过程,从而就可以利用纳米颗粒的尺寸效应实现低温连接。

本文采用脉冲激光沉积技术,避开了传统化学法所需的有机物,成功制备了 Ag-10%Pd 纳米合金(合金中钯的质量分数为 10%),并将其用于 SiC 芯片的封装互连。本文研究了沉积态和烧结态 Ag-10%Pd 纳米合金的微观组织,分析了烧结温度对接头剪切性能的影响。此外,还讨论了 Ag-10%Pd 纳米合金的抗电化学迁移过程,并将其与纯银进行了对比分析。

2 试验方法

采用脉冲激光沉积技术制备 Ag-10%Pd 纳米合金,如图 1(a)所示。所用皮秒激光的单脉冲能量

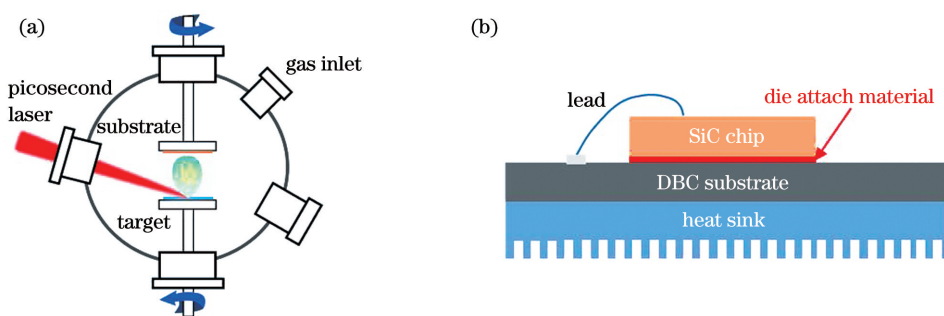


图 1 纳米合金的制备及接头截面示意图。(a)脉冲激光沉积制备纳米合金;(b)SiC 与 DBC 基板封装接头截面
Fig. 1 Schematic illustration of nanoalloy preparation and joint cross-section. (a) Pulsed laser deposition of nanoalloy;
(b) cross-section of SiC and DBC substrate joint

电化学迁移测试方法采用经典的水滴试验。电极所在基板为 Al_2O_3 ,在距离 1 mm 的两电极之间滴加去离子水,并加载 5 V 电压,以短路电流达到 1 mA 所用时间作为两片电极被迁移产物短路的时间。

3 试验结果与讨论

3.1 沉积态 Ag-10%Pd 纳米合金的表征

沉积态 Ag-10%Pd 纳米合金薄膜如图 2(a)所示。在已有脉冲激光沉积制备 Ag-Cu 纳米合金的工艺基础上^[15],本文通过控制沉积时间,成功制备出厚度约为 85 μm 的纳米合金薄膜。由于脉冲激光沉积为纯物理手段,因此完全避免了传统化学手段常用的有机物,为后续烧结奠定了良好的基础。图 2(c)、(d)所示为沉积态纳米合金颗粒的元素分布,可以看出,脉冲激光沉积制备的 Ag-10%Pd 纳米颗粒中的元素分布均匀,纳米颗粒均以合金的形式存在。在本文制备的 Ag-10%Pd 纳米合金中,钯的质量分数为 9.7%,与靶材中钯的质量分数(10%)相吻合。根据 Ag-Pd 相图^[16-17],银、钯二者

为 200 μJ ,波长为 1064 nm,脉宽为 10 ps,靶材与基板的转速均为 60 r/min。封装连接所用芯片为 SiC 芯片,基板为镀银的直接覆铜基板(DBC)。纳米颗粒沉积在 SiC 芯片背面,然后将芯片转移到 DBC 基板上进行烧结与后续表征,接头截面示意图如图 1(b)所示。选取 5 张不同视野下的典型扫描电镜图像统计沉积态 Ag-10%Pd 纳米合金颗粒的直径。假定纳米颗粒都是规则的球形,对纳米颗粒直径进行统计,得到不同粒径颗粒的数量比和体积比。烧结温度为 200~350 $^{\circ}\text{C}$,时间为 30 min,压力为 5 MPa。Ag-10%Pd 靶材中银和钯的质量比为 90:10。此外,为与 Ag-Pd 进行对比,本文沉积了纯银薄膜,沉积参数与上述参数一致。

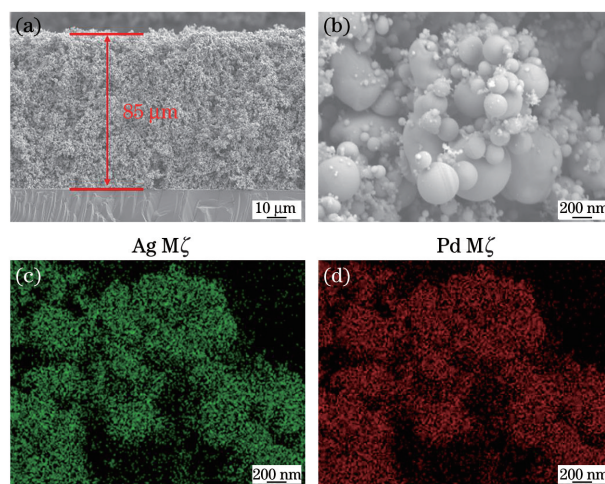


图 2 沉积态 Ag-10%Pd 纳米合金薄膜。(a)Ag-10%Pd 纳米合金薄膜;(b)Ag-10%Pd 纳米合金的高倍形貌;(c)合金颗粒中银元素的分布;(d)合金颗粒中钯元素的分布
Fig. 2 As-deposited Ag-10%Pd nanoalloy film. (a) Ag-10%Pd nanoalloy film; (b) high magnification of Ag-10%Pd nanoalloy; (c) element distribution of Ag in nanoalloy; (d) element distribution of Pd in nanoalloy

完全互溶,而脉冲激光具有保组分的特性,因此能够成功制备 Ag-10%Pd 纳米合金。

沉积态 Ag-10%Pd 纳米合金薄膜由无数纳米颗粒组成。不同粒径颗粒的数量分布及体积比如图 3 所示,其中曲线为变化趋势的拟合。可以看出,99%的纳米颗粒粒径均小于 $1\ \mu\text{m}$,其中又以直

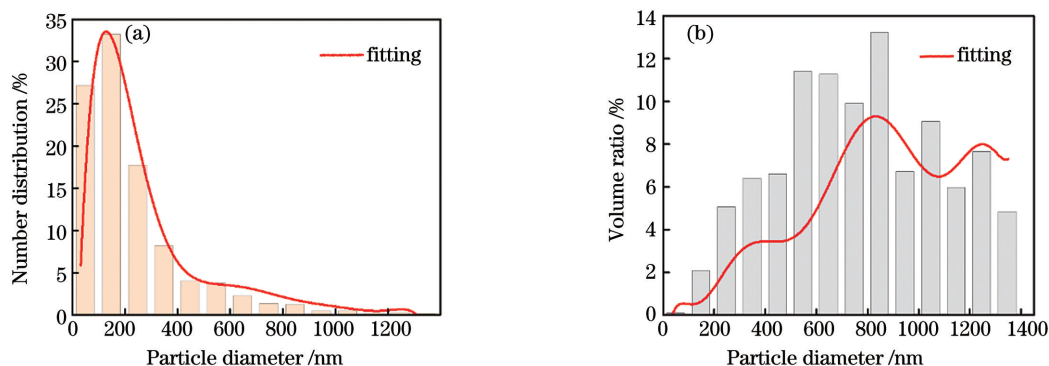


图 3 Ag-10%Pd 纳米合金颗粒的尺寸分布。(a)数量分布;(b)体积比

Fig. 3 Size distribution of Ag-10%Pd nanoalloy particles. (a) Number distribution; (b) volume ratio

3.2 Ag-10%Pd 纳米合金烧结接头的微观组织

将沉积态 Ag-10%Pd 纳米合金薄膜用于 SiC 芯片与镀银 DBC 的互连,典型的烧结接头(烧结温度为 $300\ \text{C}$)截面及元素分布如图 4 所示。烧结接头由三部分构成,自上而下分别是背面带有磁控溅射银层(厚约为 $1\ \mu\text{m}$)的 SiC 芯片、Ag-Pd 合金烧结层以及正面带有镀银层(约为 $10\ \mu\text{m}$)的 DBC 基板。

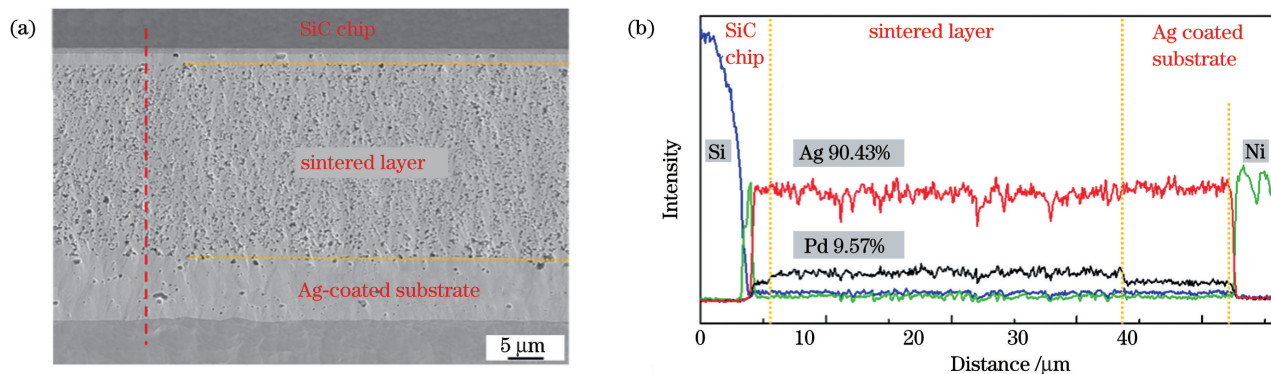


图 4 Ag-10%Pd 纳米合金烧结接头及接头中的元素分布(烧结温度为 $300\ \text{C}$)。(a)接头的宏观形貌;(b)元素线扫描

(a) Macro morphology of joint; (b) elements distribution by line scanning

典型 Ag-10%Pd 纳米合金烧结层(烧结温度为 $300\ \text{C}$)的微观组织及元素分布如图 5 所示。在烧结过程中,小的纳米颗粒由于 Ostwald 效应被大颗粒吞并^[18-20];在表面扩散以及体积扩散等多种扩散机制的作用下,大颗粒间形成烧结颈,并随着烧结的推进发生致密化。尽管烧结组织发生了明显变化,但烧结层截面上的银、钯元素仍然分布均匀,未发生

径为 $150\ \text{nm}$ 的颗粒居多。与块体材料相比,这些纳米尺度的合金颗粒具有非常高的表面能,在压力的辅助下能够在远低于块体材料熔点的温度下实现烧结连接。这也是激光沉积 Ag-Pd 纳米合金烧结与银、钯颗粒直接混合烧结、合金化相比所具有的不可替代的优势。

烧结层上下互连界面均无裂纹出现,成功实现了二者的可靠互连。烧结层的厚度约为 $27\ \mu\text{m}$,仅为沉积态薄膜厚度的 31.6% ,说明本文采用脉冲激光沉积工艺制备的合金薄膜具有非常高的压缩性。该 Ag-10%Pd 纳米合金薄膜具有非常好的变形能力,对待连接的粗糙表面有一定的填充作用,从而降低了对连接表面粗糙度的要求。

无明显的偏聚现象,如图 5(b)、(c)所示,钯元素的质量分数约为 9.57% ,与沉积态纳米合金中钯元素的含量一致。可见,采用 Ag-Pd 纳米合金的方式添加钯元素,能够获得成分均匀的合金接头。相比于传统的银、钯颗粒直接混合的方法,激光沉积 Ag-Pd 纳米合金的烧结成功避免了高温合金化过程,能够实现 SiC 芯片的低温封装。

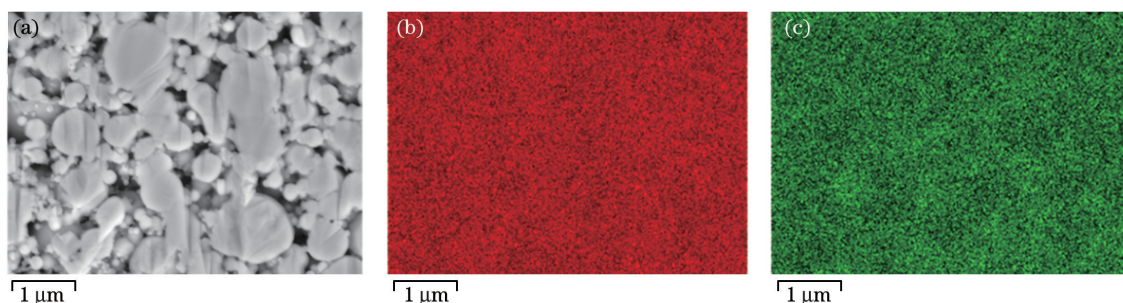


图 5 典型 Ag-10%Pd 纳米合金烧结层的微观组织及元素分布(烧结温度为 300 °C)。(a)烧结层的微观组织;(b)银元素分布;(c)钯元素分布

Fig. 5 Typical microstructures and element distribution of Ag-10%Pd sintered layer (sintering temperature of 300 °C).

(a) Microstructure of Ag-Pd sintered layer; (b) Ag distribution; (c) Pd distribution

3.3 Ag-10%Pd 纳米合金烧结接头的剪切强度

烧结温度是影响烧结程度以及为烧结提供驱动力的最重要参数之一。本文研究了烧结温度对烧结接头剪切强度的影响。如图 6 所示,当烧结温度为 200 °C 时,由于烧结不够充分,接头剪切强度低于美国军标 MIL-STD-883K^[21] 的 7.8 MPa 要求。随着烧结温度提高到 300 °C,剪切强度基本呈线性增加,并达到了 56.85 MPa,远超上述标准的要求。这说明随着温度升高,纳米合金的烧结越来越充分。当温度进一步升高到 350 °C 时,接头强度虽然仍有一定程度的提高,但提高的幅度较小。这是因为烧结组织的致密化在 300 °C 时已进行得较为充分,继续提高烧结温度所起的作用有限。

图 7 为 300 °C 烧结接头断口的宏观形貌及局部放大图。可以发现,剪切失效基本上发生在烧结层,

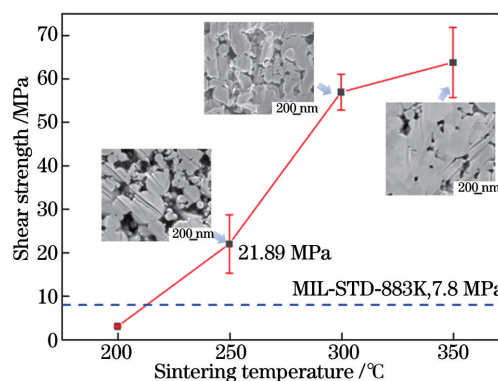


图 6 烧结温度对接头剪切强度的影响

Fig. 6 Effect of sintering temperature on joint shear strength. Shear strength increases with sintering temperature, exceeding the MIL-STD-883K requirement of 7.8 MPa. The failure is primarily observed in the Ag-Ni plating layer on the back of the chip. This indicates that the Ag-10%Pd nanoalloy thin film achieves good metallurgical bonding with the SiC back and DBC front, laying a good foundation for the reliable service of subsequent power electronic devices.

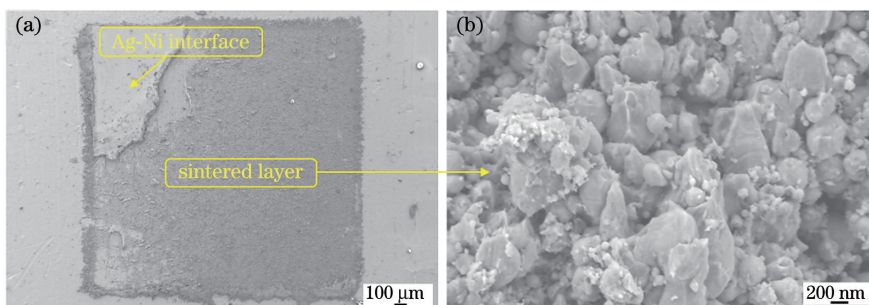


图 7 典型纳米合金烧结接头的断口形貌(烧结温度为 300 °C)。(a)断口的宏观形貌;(b)断口局部放大

Fig. 7 Typical fracture surface of nanoalloy sintered joint (sintering temperature of 300 °C). (a) Macro morphology of fracture surface; (b) high magnification of fracture surface

3.4 Ag-10%Pd 纳米合金的抗电化学迁移能力

在 5 V/mm 的电场作用下,对 Ag-10%Pd 纳米合金及纯银的抗电化学迁移能力进行测试,并实时记录电流以及电极间的形貌随通电时间的变化。如图 8 所示,对于纯银电极,在通电 65.6 s 之后,由于电极间迁移产物的导通,电流开始迅速增加,并随着

迁移产物的生长在 81.4 s 时达到短路电流 (1 mA)。对于 Ag-10%Pd 电极,电流在 228.5 s 之前都维持在非常低的水平,最终达到短路电流的时间为 349.7 s,有效工作时间大约是纯银电极的 4.3 倍。

纯银电极间的电流达到 1 mA 时(81.4 s)的电化学迁移产物如图 9(a)所示,可以发现纯银的阴极

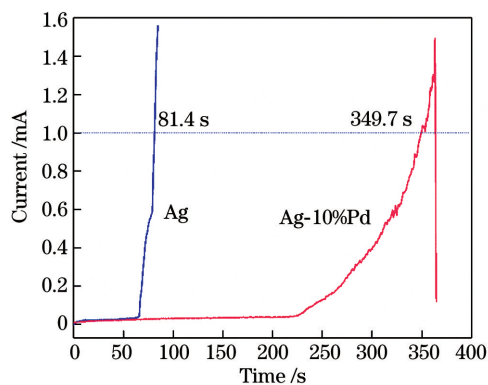


图 8 Ag-10%Pd 纳米合金与纯银的短路电流随时间的变化

Fig. 8 Short-circuit current variation with time for Ag-10%Pd nanoalloy and pure Ag

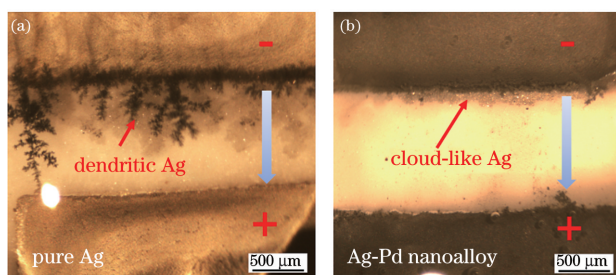


图 9 电化学迁移产物。(a) 纯银；(b) Ag-10%Pd

Fig. 9 Electrochemical-migration product. (a) Pure Ag; (b) Ag-10%Pd

上生长出了树枝状银产物,并朝向阳极生长,最终有少量生长速度较快的银产物将两电极导通,导致电流迅速增大。对于 Ag-10%Pd 纳米合金,同样有银产物在阴极上产生,但其形态呈云雾状,而且整体朝向阳极生长,银的溶解和生长受到了明显抑制。Lin 等^[10]报道过类似的现象,这是因为钯元素的添加导致合金表面生成了 PdO,阻碍了银离子的析出和迁移,降低了银离子的浓度,使得迁移产物的形貌由树枝状转变为云雾状。钯含量越高,合金电极越容易被 PdO 覆盖,即钯含量的高低直接影响了银离子析出的难易程度。

需要指出的是,块体材料钯的熔点高达 1554 °C,远高于银的熔点(961.7 °C)。钯的添加提高了银合金的熔点,使得 Ag-Pd 纳米合金的烧结相比纯银需要更高的温度。而对于功率电子器件的封装来说,烧结温度不能过高。另一方面,钯的成本也非常高。本研究提出的以脉冲激光沉积为手段制备 Ag-Pd 纳米合金以避免高温合金化过程从而降低烧结温度的思路,在实际应用中还应根据具体的应用场景,综合考虑烧结温度、抗电化学迁移要求及成本,选择具有合适成分比例的 Ag-Pd 纳米合金进行芯片的封装。

4 结 论

本文采用脉冲激光沉积成功制备了完全互溶的 Ag-10%Pd 纳米合金,其烧结接头组织为元素均匀分布的 Ag-Pd 固溶体。相比于银、钯纳米颗粒直接混合烧结,脉冲激光沉积 Ag-Pd 纳米合金的烧结避免了高温合金化过程,实现了不高于 300 °C 的低温封装互连。

Ag-10%Pd 纳米合金作为封装互连材料,在 250 °C 的烧结连接条件下可以获得剪切强度为 21.89 MPa 的接头,超过了美国军标 MIL-STD-883K 的要求(7.8 MPa);进一步提高烧结温度到 300 °C,接头的剪切强度可达到 56.85 MPa。接头的失效发生在烧结层,说明 Ag-10%Pd 纳米合金烧结实现了高质量的界面连接。

Ag-10%Pd 纳米合金的抗电化学迁移能力是同条件下纯银的 4.3 倍。Ag-10%Pd 纳米合金表面的 PdO 阻碍了银离子的析出,迁移产物的生长受到抑制并呈云雾状分布,有效延长了电极的短路时间。

致谢 本研究得到了清华大学机械工程系邹贵生教授的大力支持和指导。

参 考 文 献

- [1] Ni Y X, Jing H Q, Kong J X, et al. Thermal performance of high-power laser diodes packaged by SiC ceramic submount [J]. Chinese Journal of Lasers, 2018, 45(1): 0101002.
倪羽茜, 井红旗, 孔金霞, 等. 碳化硅封装高功率半导体激光器散热性能研究 [J]. 中国激光, 2018, 45(1): 0101002.
- [2] Zhang B, Deng X C, Zhang Y R, et al. Recent development and future perspective of silicon carbide power devices: opportunity and challenge [J]. Journal of China Academy of Electronics and Information Technology, 2009, 4(2): 111-118.
张波, 邓小川, 张有润, 等. 宽禁带半导体 SiC 功率器件发展现状及展望 [J]. 中国电子科学研究院学报, 2009, 4(2): 111-118.
- [3] Wang T, Chen X, Lu G Q, et al. Low-temperature sintering with nano-silver paste in die-attached interconnection [J]. Journal of Electronic Materials, 2007, 36(10): 1333-1340.
- [4] Zhu Y, Tang S P, Yan J F, et al. Comparison of the bonding through sintering between Ag nanoparticle paste and Ag microparticle paste [J]. Journal of Beijing University of Aeronautics and

- Astronautics, 2013, 39(4): 484-487.
朱颖, 唐善平, 闫剑锋, 等. 纳米银膏与微米银膏烧结连接对比[J]. 北京航空航天大学学报, 2013, 39(4): 484-487.
- [5] Mu F W, Zou G S, Zhao Z Y, et al. Low temperature sintering-bonding through *in situ* formation of Ag nanoparticles using micro-scaled Ag₂O composite paste[J]. Transactions of the China Welding Institution, 2013, 34(4): 38-42, 115.
母凤文, 邹贵生, 赵振宇, 等. 微米氧化银膏原位生成纳米银的低温烧结连接[J]. 焊接学报, 2013, 34(4): 38-42, 115.
- [6] Stukowski A. Visualization and analysis of atomistic simulation data with OVITO—the Open Visualization Tool [J]. Modelling and Simulation in Materials Science and Engineering, 2010, 18(1): 015012.
- [7] Mei Y H. The investigation of low temperature sintered nanosilver paste on migration and thermal bending in die-attachment [D]. Tianjin: Tianjin University, 2010.
梅云辉. 低温烧结纳米银焊膏电迁移和粘接热弯曲性能研究[D]. 天津: 天津大学, 2010.
- [8] Kim K S, Jung K H, Park B G, et al. Characterization of Ag-Pd nanocomposite paste for electrochemical migration resistance [J]. Journal of Nanoscience and Nanotechnology, 2013, 13(11): 7620-7624.
- [9] Naguib H, MacLaurin B. Silver migration and the reliability of Pd/Ag conductors in thick-film dielectric crossover structures [J]. IEEE Transactions on Components, Hybrids, and Manufacturing Technology, 1979, 2(2): 196-207.
- [10] Lin J C, Chan J Y. On the resistance of silver migration in Ag-Pd conductive thick films under humid environment and applied d.c. field [J]. Materials Chemistry and Physics, 1996, 43(3): 256-265.
- [11] Wang D. On resistance of nano-Ag-Pd paste to electrochemical migration behavior at high temperatures[D]. Tianjin: Tianjin University, 2018.
王迪. 高温环境下纳米 Ag-Pd 焊膏的抗电化学迁移老化行为研究[D]. 天津: 天津大学, 2018.
- [12] Lin J C, Wu W. On the sintering of mixed and alloyed silver-palladium powders from chemical coprecipitation[J]. Materials Chemistry and Physics, 1995, 40(2): 110-118.
- [13] Buttay C, Planson D, Allard B, et al. State of the art of high temperature power electronics [J]. Materials Science and Engineering B, 2011, 176(4): 283-288.
- [14] Feng B, Shen D Z, Wang W G, et al. Cooperative bilayer of lattice-disordered nanoparticles as room-temperature sinterable nanoarchitecture for device integrations [J]. ACS Applied Materials & Interfaces, 2019, 11(18): 16972-16980.
- [15] Jia Q, Zou G S, Wang W G, et al. Sintering mechanism of a supersaturated Ag-Cu nanoalloy film for power electronic packaging [J]. ACS Applied Materials & Interfaces, 2020, 12(14): 16743-16752.
- [16] Kim D H, Kim H Y, Ryu J H, et al. Phase diagram of Ag-Pd bimetallic nanoclusters by molecular dynamics simulations: solid-to-liquid transition and size-dependent behavior [J]. Physical Chemistry Chemical Physics, 2009, 11(25): 5079-5085.
- [17] Karakaya I, Thompson W T. The Ag-Pd (silver-palladium) system [J]. Bulletin of Alloy Phase Diagrams, 1988, 9(3): 237-243.
- [18] Ji Y T, Yang S C, Guo S W, et al. Bimetallic Ag/Au nanoparticles: a low temperature ripening strategy in aqueous solution [J]. Colloids and Surfaces A: Physicochemical and Engineering Aspects, 2010, 372(1/2/3): 204-209.
- [19] Anderson R, Buscall R, Eldridge R, et al. Ostwald ripening of comb polymer stabilised Ag salt nanoparticles [J]. Colloids and Surfaces A: Physicochemical and Engineering Aspects, 2014, 459: 58-64.
- [20] Tian Y H, Jiang Z, Wang C X, et al. Sintering mechanism of the Cu-Ag core-shell nanoparticle paste at low temperature in ambient air [J]. RSC Advances, 2016, 6(94): 91783-91790.
- [21] United States Department of Defense. Test method standard: microcircuits: MUL-STD_883K [S/OL]. [2020-11-30]. <http://www.everyspec.com>.

Low-Temperature Bonding of Ag-Pd Nanoalloy and Its Resistance to Electrochemical-Migration

Jia Qiang, Wang Wengan, A Zhanwen, Deng Zhongyang, Feng Bin, Liu Lei*

Department of Mechanical Engineering, State Key Laboratory of Tribology, Tsinghua University, Beijing 100084, China

Abstract

Objective There is an increasing demand for die attach materials with the rapid development of SiC devices, which can be bonded at low-temperature and function at high temperature. Nano-Ag sintering has been extensively investigated for application in high-temperature power electronics. However, the electrochemical-migration of Ag ions is the main drawback. Pd is famous for its chemical stability, and various studies have focused on the influence of Pd content on the effectiveness and its mechanism. Recently, researchers have been trying to mix Pd and Ag nanoparticles (NPs) to improve the resistance to electrochemical-migration of the sintered layer. However, Pd has a melting point higher than that of Ag, whereas the alloying process needs high temperature ($\sim 850\text{ }^{\circ}\text{C}$) to form Ag-Pd alloy. Pulsed laser deposition (PLD) is a physical method feasible for fabricating Ag-Pd nanoalloy without using organic additives such as polyvinylpyrrolidone, which is required in the chemical method. In this work, Ag-10%Pd nanoalloy was fabricated by the PLD method, which can be used to connect SiC and Ag-coated direct bonding copper (DBC) substrates. The sintered layer enhances resistance to electrochemical-migration with low-temperature bonding characteristics. The microstructure of the bonding, shear properties, and its electrochemical-migration resistance are studied.

Methods Ag-10%Pd NPs were fabricated using PLD with a pressure of 750 Pa of Ar atmosphere. The Ag-Pd target was fabricated by powder sintering with weight ratio of 90 : 10. A picosecond laser with a pulse width of 10 ps was employed to ablate the target. Ag-Pd NPs were deposited on the back side of SiC chip (G. P. Tech, Ti/Ni/Ag metallization), then the SiC chip was removed from the substrate and placed on the Ag-coated DBC (HuaSemi Electronics, Ni/Au metallization). The interconnecting process is performed at a temperature range of $200\text{ }^{\circ}\text{C}$ – $350\text{ }^{\circ}\text{C}$ assisted with a pressure of 5 MPa for 30 min in air. The shear test is conducted using Dage 4000. The electrochemical-migration test is conducted using a water drop test.

Results and Discussions The microstructure of as-deposited Ag-Pd film comprises various NPs with diameters less than $1\text{ }\mu\text{m}$ (Fig. 3). Element results indicate that these deposited NPs are in alloy state with a uniform composition distribution. The sintered joint comprises SiC chip, bondline and Ag-coated substrates (Fig. 4). The bondline thickness is about $27\text{ }\mu\text{m}$, which is only 31.6% of the as-deposited state. Thus, the Ag-Pd film had excellent deformability. The bondline exhibited Ag-9.57%Pd alloy microstructure without obvious element segregation. The sintered joint achieved a shear strength of 21.89 MPa at the sintering temperature of $250\text{ }^{\circ}\text{C}$, which is higher than the US military standard MIL-STD-883K (7.8 MPa). Therefore, Ag-Pd nanoalloy film can be used as die attach material for low-temperature bonding. The sintering temperature provides the driving force for sintering process, as a denser bondline is achieved when the temperature is increased to $300\text{ }^{\circ}\text{C}$ (Fig. 6). Fracture surface reveals that the failure mainly occurred at the bondline, indicating that high bonding quality interface is realized (Fig. 7). Compared with pure Ag, Ag-Pd nanoalloy exhibited a more than quadruple resistance to electrochemical-migration during the water drop test (Fig. 8). For pure Ag electrode, the current reached 1 mA with only 81.4 s, while the Ag-Pd electrode required 349.7 s for the short-circuit process. The dissolution of Ag ion was blocked by PdO formation on the anode, which played a paramount role in extending the short-circuit time, whereas the migration product was cloud-like instead of dendritic growth. This work proposed a method for fabricating Ag-Pd nanoalloy films as die attach material without the high alloying temperature. It should be noted that, Pd has a higher melting point ($1554\text{ }^{\circ}\text{C}$) than Ag ($961.7\text{ }^{\circ}\text{C}$), and Ag-Pd nanoalloy sintering requires higher sintering temperature than pure Ag NPs. Moreover, adding Pd is costly. Consequently, the sintering temperature, demand of electrochemical-migration resistance and its cost should be balanced when applying Ag-Pd nanoalloy in electronic packaging.

Conclusions Ag-10%Pd nanoalloy was successfully fabricated as die attach material using PLD. The sintered joint

achieved a shear strength of 21.89 MPa at the sintering temperature of 250 °C, which was higher than the US military standard MIL-STD-883K (7.8 MPa). Compared with pure Ag, Ag-Pd nanoalloy exhibited a more than quadruple electrochemical-migration resistance. The dissolution of Ag ion was blocked by PdO formation on the anode with obviously extended short-circuit time, whereas the migration product was cloud-like. Compared with conventional direct sintering of Ag and Pb nanoparticles, pulsed laser deposited Ag-Pd nanoalloy sintering avoids high-temperature alloying process (850 °C), which is promising for Ag-Pd low-temperature bonding and is expected to provide a solution for the high-reliability power electronic packaging.

Key words laser technique; nanoalloy; low-temperature sintering; electronic packaging; electrochemical-migration

OCIS codes 160.4236; 140.7090; 160.3900